ASM–FDTD: A Technique for Calculating the Field of a Finite Source in the Presence of an Infinite Periodic Artificial Material

Rui Qiang, Ji Chen, Filippo Capolino, David R. Jackson, and Donald R. Wilton

***Abstract*—A novel technique is proposed to calculate the field due to an arbitrary impressed source of finite extent in proximity with an infinite periodic structure such as an artificial material. The algorithm is based on a spectral domain finite-difference time-domain (FDTD) method combined with the array scanning method (ASM). Using this approach, only a single periodic cell of the periodic structure needs to be numerically modeled. Examples are used to demonstrate the accuracy and efficiency of the proposed approach.**

***Index Terms*—Arrays, artificial materials, finite-difference time-domain (FDTD), finite source, Green's function, metamaterials, periodic structures.**

I. Introduction

PERIODIC structures such as frequency selective surfaces, electromagnetic bandgap materials, metamaterials, and guiding periodic structures are topics that now receive a lot of attention in both the optics and microwave communities. However, the time-domain (TD) modeling of impressed electromagnetic sources of finite extent in proximity with infinite periodic structures has been to date performed by "brute force," including a large number of unit cells in the simulation domain [1], which requires extensive computational resources. This letter presents a novel TD technique to model the excitation of infinite periodic structures with a finite source. For simplicity, the discussion here is restricted to structures that are periodic in one dimension and are excited by a line source, but the extension to structures that are periodic in 2-D and are excited by finite (e.g., dipole) sources can readily be done. This method is based on the combination of the array scanning method (ASM) [2]–[5] and the spectral-domain FDTD method [6]–[11]. Accordingly, the spectral FDTD method is applied here to only one unit cell, with proper complex periodic boundary conditions, accounting for the impressed line source. The FDTD with complex periodic boundary conditions, used in the spectral FDTD, is different from the traditional delay boundary conditions used in other periodic FDTD methods [12], [13]. No field transformation is necessary in this method and the stability condition of this method is no longer limited by the angle of incidence.

Manuscript received September 28, 2006; revised December 6, 2006.

R. Qiang, J. Chen, D. R. Jackson, and D. R. Wilton are with the Department of Electrical and Computer Engineering, University of Houston, Houston, TX 77204-4005 USA (e-mail: jchen18@uh.edu).

F. Capolino is with the Department of Electrical and Computer Engineering, University of Houston, Houston, TX 77204-4005 USA and also with the Department of Information Engineering, University of Siena, Siena 53100, Italy (e-mail: capolino@dii.unisi.it).

Digital Object Identifier 10.1109/LMWC.2007.892964

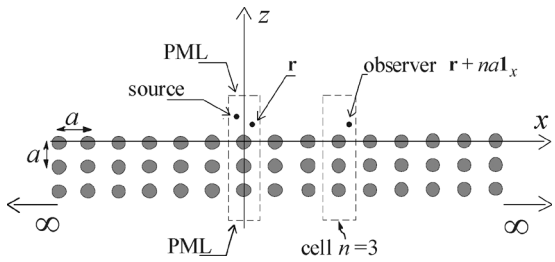

Fig. 1. Geometry of a line source over a periodic artificial material made of conducting cylinders. The period along x is denoted by a. The dashed line around the origin represents the FDTD computation domain with complex periodic boundary conditions (4) along x, and perfect matching layers (PML) on the top and bottom.

II. ASM–FDTD Method

Consider, as an example, the structure in Fig. 1, where a is the period along x and r_0 is the location of the electric line source that produces an electric field E_y, which is henceforth referred to simply as E. The observation point in an arbitrary periodic nth cell (Fig. 1) is denoted by $r + na1_x$, where r is defined in the $n = 0$ periodic cell, and 1_x is the unit vector along x. (The source and observation points are vectors, although vector notation is being suppressed here.) In the frequency domain, an $e^{j\omega t}$ time-dependence is assumed and suppressed, and the ASM representation of the total field at $r + na1_x$, produced by the single source in the periodic environment is [3]

$$E_{tot}(r+na1_x, r_0, \omega) = \frac{a}{2\pi} \int_{-\pi/a}^{\pi/a} E_{tot}^{\infty}(r, r_0, k_x, \omega) e^{-jk_x na} dk_x. \tag{1}$$

In (1), $E_{tot}^{\infty}(r, r_0, k_x, \omega)$ is the electric field at r in the infinite periodic structure produced by a periodic set of sources at $r_0 + ma1_x$ $(m = 0, \pm 1 \ldots)$, with a phase shift $\exp(-jk_x a)$ between adjacent sources. This creates a periodic problem in which there is a phase shift $\exp(-jk_x a)$ between the left and right periodic boundaries in Fig. 1. The electromagnetic fields in the periodic structure therefore satisfy periodic boundary conditions. For example, the electric field satisfies

$$E_{tot}^{\infty}(r + a1_x, r_0, k_x, \omega) = E_{tot}^{\infty}(r, r_0, k_x, \omega) e^{-jk_x a}. \tag{2}$$

The integration domain in (1) is often denoted as the fundamental Brillouin zone. The TD counterpart of (1) comes from

taking an inverse Fourier transform of it and then reversing the order of the integration in k_x and ω. The result is

$$\hat{E}_{tot}(r+na1_x, r_0, t) = \frac{a}{2\pi} \int_{-\pi/a}^{\pi/a} \hat{E}^{\infty}_{tot}(r, r_0, k_x, t) e^{-jk_x na} dk_x \tag{3}$$

where the hat ˆ denotes TD quantities. Here, in the time domain (3), just as in the frequency domain (2), the field quantities are complex and a periodic boundary condition at the edges of the unit cell are assumed, corresponding to the wavenumber k_x. For example, the electric field $\hat{E}^{\infty}_{tot}$ satisfies the inverse Fourier transform of (2), which is

$$\hat{E}^{\infty}_{tot}(r + a1_x, r_0, k_x, t) = \hat{E}^{\infty}_{tot}(r, r_0, k_x, t) e^{-jk_x a}. \tag{4}$$

Equation (4) makes it obvious that in this rather unusual TD application, the TD field $\hat{E}^{\infty}_{tot}(r, r_0, k_x, t)$ is a complex function. The same periodicity condition in the TD has been used already in [9]–[11].

To implement the periodic boundary condition (4) using the FDTD method, the phasing parameter k_x has been discretized in an even number N_{kx} of spectral sampling points, uniformly distributed over the fundamental Brillouin zone. Spectral FDTD simulations are carried out at every spectral sampling point using the boundary condition described by (4) [10]. Since complex values described in (4) are used in the FDTD implementation, both electric and magnetic values are complex. For every spectral sampling point $k_x = \xi_i = \pi a^{-1}[-1 + (2i-1)/N_{kx}]$, with $i = 1, \ldots, N_{kx}$, the computed field $\hat{E}^{\infty}_{tot}(r, r_0, \xi_i, t)$ is obtained. For simplicity, we use the simple midpoint rectangle rule of integration, which is particularly effective for smooth periodic functions [14]

$$\hat{E}_{tot}(r+na1_x, r_0, t) = \frac{1}{N_{kx}} \sum_{i=1}^{N_{kx}} \hat{E}^{\infty}_{tot}(r, r_0, \xi_i, t) e^{-jna\xi_i} \tag{5}$$

though other schemes may be more appropriate if the integrand is singular. It should be pointed out that if a real-value excitation term is used, the final value of (5) is also real-valued. The detailed implementation of the spectral FDTD is as in [9]–[11].

III. Illustrative Examples

To validate the method and test the accuracy and convergence of this algorithm, we first simulate a case where an electric line source along the y direction is located at the origin of the x–z plane in a free-space environment at a frequency of 3 GHz. In Fig. 2, the magnitude of the electric field is evaluated on a line along the x direction, with $z = 0$, showing a good agreement between the ASM–FDTD method and the reference analytic solution. The ASM–FDTD solution is evaluated by using $N_{kx} = 30$ spectral sampling points in (5). The ASM is implemented assuming a virtual periodicity $a = 0.4\lambda$ in the x direction. The FDTD Yee cell size here and in the next example is $\Delta x = \Delta z =$ 1 mm. To further study the convergence of this method, the numerical error defined as

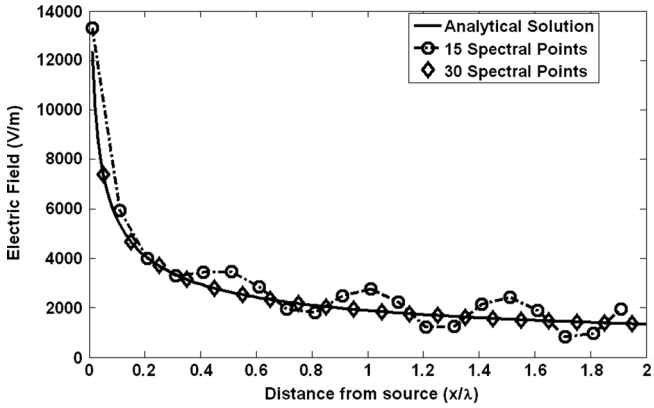

Fig. 2. Electric field evaluated along the x axis.

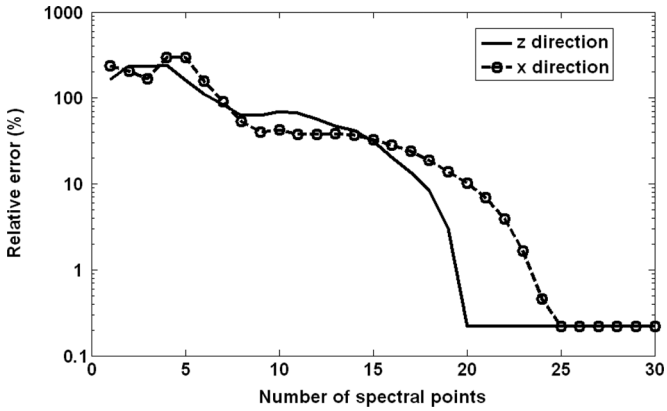

Fig. 3. Percentage relative error in the field averaged along a line between $0.5a$ and $1.5a$, oriented in either the x or z direction.

$$\text{Error}\% = \frac{\sqrt{\int_{0.5a}^{1.5a} \left[E_{\text{ASM-FDTD}}(r) - E_{\text{analytical}}(r)\right]^2 d\ell}}{\sqrt{\int_{0.5a}^{1.5a} \left[E_{\text{analytical}}(r)\right]^2 d\ell}} \times 100 \tag{6}$$

is shown in Fig. 3 versus the number of spectral points N_{kx} in (5). The error is evaluated along the line $\ell 1_u$, with $\ell \in [0.5a, 1.5a]$ and 1_u equal to either 1_x and 1_z. As clearly seen in the figure, the numerical error decreases as N_{kx} increases. In addition, the convergence rates in the x and z directions are different—the numerical result converges faster along the z direction.

Using the developed software, we now investigate the electromagnetic field behavior in the vicinity of a line source residing above an EBG material made by three rows of conducting wires as shown in Fig. 1. The wires have diameter $D = 7.2$ mm and spacing $a = 18$ mm in both the x and z directions. Fig. 4 shows the electric field (magnitude of y component) produced by a line source located at $r_0 = 0.5a1_z$, i.e., a distance $0.5a$ above the axis of the first row of wires (Fig. 1) for a frequency of 5 GHz. The field does not penetrate through the material since it has a bandgap for frequencies $f \in$ [0,8] GHz [4]. The

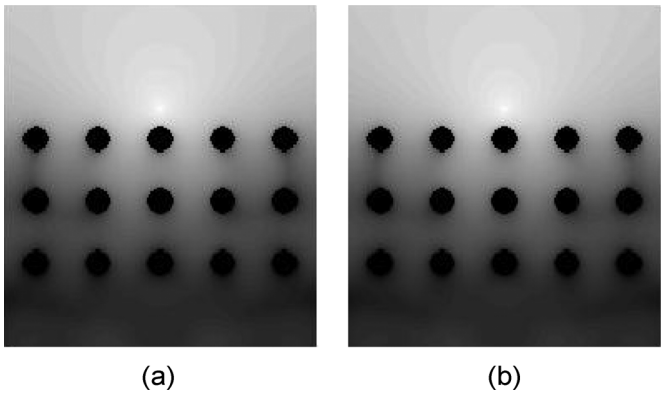

Fig. 4. Electric field distribution produced by a line source in the vicinity of an EBG material obtained by using (a) the standard FDTD method and (b) the ASM–FDTD method.

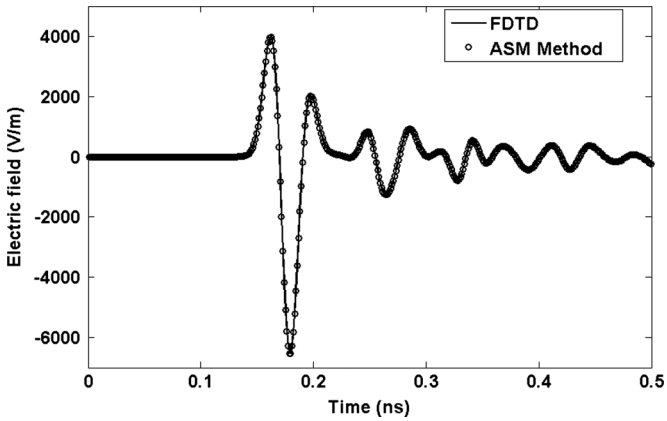

Fig. 5. TD electric field produced by a pulsed line source, evaluated at $r_0 + 2a1_x$, via the ASM–FDTD method and the standard FDTD algorithm.

FDTD Yee cell size is now given by $\Delta x = \Delta z = 0.5$ mm. Fig. 4 shows a comparison between results obtained using both the standard FDTD method [Fig. 4(a)] and the ASM–FDTD [Fig. 4(b)] where $N_{kx} = 24$ spectral points have been used in (5). As seen from the figure, these results are in good agreement with each other and the relative error is only 0.98%, where the error is defined similarly as in (6) by an average over a computation space within $x \in [-3a, 3a]$ and $z \in [0{,}5.6a]$. However, to produce the result using the FDTD method, 21 periodic cells along the x direction needed to be included in the simulation domain—otherwise truncation effects would be visible. As a consequence, the standard FDTD method requires over $10\times$ more computer memory. The solution time for this particular example is 29 s (FDTD) and 62 s (ASM–FDTD), respectively. To obtain more accurate results in regions further away from the source (not shown in Fig. 4), the FDTD method requires even larger computational domains. If 50 periodic cells are used along the x direction, the FDTD method requires $25\times$ more computer memory than that of the ASM–FDTD method. It also requires 73 s in CPU time.

In Fig. 5, the ASM–FDTD is also used to compute a transient signal for the same geometry as in Fig. 4. A Gaussian current pulse, $I(t) = I_0 \exp[-(t - t_0)^2/2\sigma_t^2]$, with $I_0 = 1$ A, $t_0 = 8.1727$ ps, and $\sigma_t = 4.9036$ ps, is now used as excitation. The transient field at $r_0 + 2a1_x$ evaluated via the ASM–FDTD by using $N_{kx} = 24$ spectral points in (5), is in good agreement with the field obtained via the standard FDTD method.

IV. Conclusion

A time-domain version of the ASM has been presented for the first time. This algorithm allows for the solution of a finite-size source excitation of an infinite periodic structure in the time domain. Only a single unit cell needs to be discretized. The algorithm has been implemented by using the spectral FDTD method for complex signals, which is particularly suitable for stable FDTD methods involving incidence angles near grazing, showing good agreement with a reference solution. The memory usage of this ASM–FDTD method is drastically reduced compared to a standard FDTD implementation, which has to discretize a large portion of the periodic structure to avoid truncation effects.

References

[1] C. Luo, S. G. Johnson, and J. D. Joannopoulos, "All-angle negative refraction without negative effective index," *Phys. Rev. Rapid Commun.*, vol. B65, p. 201104(R), 2002.

[2] C. P. Wu and V. Galindo, "Properties of a phased array of rectangular waveguides with thin walls," *IEEE Trans. Antennas Propag.*, vol. AP-14, no. 3, pp. 163–173, Mar. 1966.

[3] B. A. Munk and G. A. Burrell, "Plane-wave expansion for arrays of arbitrarily oriented piecewise linear elements and its application in determining the impedance of a single linear antenna in a lossy half-space," *IEEE Trans. Antennas Propag.*, vol. AP-27, no. 5, pp. 331–343, May 1979.

[4] F. Capolino, D. R. Jackson, and D. R. Wilton, "Mode excitation from sources in two-dimensional PBG waveguides using the array scanning method," *IEEE Microw. Wireless Compon. Lett.*, vol. 15, no. 2, pp. 49–51, Feb. 2005.

[5] ——, "Fundamental properties of the field at the interface between air and a periodic artificial material excited by a line source," *IEEE Trans. Antennas Propag.*, vol. 53, no. 1, pp. 91–99, Jan. 2005.

[6] A. C. Cangellaris, M. Gribbons, and G. Sohos, "A hybrid spectral/FDTD method for the electromagnetic analysis of guided waves in periodic structures," *IEEE Microw. Guided Wave Lett.*, vol. 3, no. 10, pp. 375–377, Oct. 1993.

[7] A. Aminian and Y. Rahmat-Samii, "Bandwidth determination for soft and hard ground planes by spectral FDTD: A unified approach in visible and surface waver regions," *IEEE Trans. Antennas Propag.*, vol. 53, no. 6, pp. 18–28, Jan. 2005.

[8] ——, "Spectral FDTD: A novel technique for the analysis of oblique incident plane wave on periodic structures," *IEEE Trans. Antennas Propag.*, vol. 54, no. 6, pp. 1818–1825, Jun. 2006.

[9] T. Kokkinos, C. D. Sarris, and G. V. Eleftheriades, "Periodic FDTD analysis of leaky-wave structures and applications to the analysis of negative-refractive-index leaky-wave antennas," *IEEE Trans. Microw. Theory Tech.*, vol. 54, no. 4, pp. 1619–1630, Apr. 2006.

[10] F. Yang, J. Chen, R. Qiang, and A. Elsherbeni, "FDTD analysis of periodic structures at arbitrary incidence angles: A simple and efficient implementation of the periodic boundary conditions," in *Proc. IEEE Antennas Propag. Soc. Int. Symp.*, Jun. 2006, pp. 2715–2718.

[11] R. Qiang, J. Chen, and F. Yang, "FDTD simulation of infrared FSS transmission spectrum from oblique incidence," in *Proc. IEEE Antennas Propag. Soc. Int. Symp.*, Jun. 2006, pp. 4179–4182.

[12] H. Holter and H. Steyskal, "Infinite phased-array analysis using FDTD periodic boundary conditions-pulse scanning in oblique directions," *IEEE Trans. Antennas Propag.*, vol. 10, no. 10, pp. 1508–1514, Oct. 1999.

[13] M. Turner and C. Christodoulou, "FDTD analysis of phased array antennas," *IEEE Trans. Antennas Propag.*, vol. 47, no. 4, pp. 661–667, Apr. 1999.

[14] J. A. C. Weideman, "Numerical integration of periodic functions: A few examples," *Amer. Math. Month.*, vol. 109, no. 11, pp. 21–36, Jan. 2002.